Ceram. Eng. Sci. Proc., 9 [9-10] pp. 1343-1354 (1988)

Crystallization and Characterization of Y_2O_3-SiO_2 Glasses

C. H. DRUMMOND III AND W. E. LEE
The Ohio State University
Columbus, OH

W. A. SANDERS AND J. D. KISER
NASA Lewis Research Center
Cleveland, OH

Results of crystallization studies on glasses with 20-40 mol% Y_2O_3 in the Y_2O_3-SiO_2 system are presented. Glasses were melted in W crucibles at 1900°C-2100°C in 1 and 50 atm N_2. Phase identification by X-ray diffraction and TEM indicated crystallization of the δ, γ, γ′ and β-$Y_2Si_2O_7$, depending on melting and quenching conditions. Characterization of glasses was by differential thermal analysis (DTA), thermal gravimetric analysis (TGA) and chemical analysis including energy dispersive spectroscopy in the TEM. Heat treatment in an air atmpsohere from 1100°-1600°C increased the amount of crystallization and resulted in formation of Y_2SiO_5, cristobalite and polymorphs of $Y_2Si_2O_7$. The effect of 5 and 10 wt% ZrO_2 additions on crystallization was also studied.

Introduction

The use of high-temperature materials in applications such as gas turbine engines requires that the material not only be able to withstand the high temperatures, but also maintain acceptable mechanical properties during use at these temperatures, but also maintain acceptable nechamical properties during use at these temperatures or in cycling to these temperatures. Silicon nitride continues to receive extensive study as one possible material. We report here results on the crystallization of bulk glasses similar in composition to those found in the intergranular glassy grain boundary phases of sintered silicon nitride with yttria as the sintering aid. The silicon nitride composition studied contained a 6% by weight addition of Y_2O_3 to the starting silicon nitride powder as processed by NASA Lewis.[1] This composition lies in the Si_3N_4–$Y_2Si_2O_7$–Si_2N_2O triangle of the phase diagram[2] in Fig. 1. Since this powder contains silica present as a thin layer on each Si_3N_4 grain plus that resulting from addition to the starting powders or from possible oxidation during grinding, the exact composition of the intergranular glassy phase is difficult to determine.

Improvement in the high-temperature mechanical properties may result upon crystallization of a higher-melting-point crystalline phase from the glassy grain boundary phase. Crystallization of the glassy phase may be facilitated by the addition of a nucleating agent or by the alteration of the composition.

Review of Y_2O_3–SiO_2 Crystalline Phases

The diffraction data on $Y_2Si_2O_7$ crystalline polymorphs have been summarized by Liddel and Thompson.[3] A review of the available data and some

of their own indicated that there are four polymorphs: α, β, γ, and δ. The low temperature polymorph, α, transforms to β as the temperature is increased. Figure 2 gives the temperature of the transformations and the densities of the various polymorphs of $Y_2Si_2O_7$. The structure of all polymorphs consists of $Si_2O_7^{6-}$ units. The X-ray powder diffraction file indicates that there are two different patterns of the γ phase, which are designated γ (JCPDS: 20-1416) and γ' (32-1448) in this paper. There are several polymorphs of the $Y_2Si_2O_5$ phase as discussed by Liddel and Thompson.[3] The existence of the $2Y_2O_3 3SiO_2$ phase as shown in the published phase diagram[4] has not been confirmed, and, in fact, the existence of such a phase has been questioned.[3] The volume change associated with the polymorphic inversions of $Y_2Si_2O_7$ is as large as 6.7% and may be significant in the crystallization of intergranular glassy grain boundary phases in silicon nitride (see these proceedings).[5] The density of these glasses has not been reported.

Experimental Procedure

Reagent grade silica and yttrium oxide were ball milled for four hours with HSPN grinding media in dry alcohol and dried. The powder was dry milled for two hours then pressed into pellets and placed in tungsten crucibles for melting in a high-pressure nitrogen furnace.[6] Powders were melted from 1900° to 2100 °C, depending on the composition, and were held for four hours under 50 atm nitrogen. Additional melts were also made in 1 atm nitrogen. No difference in properties or crystallization behavior was observed between these two melting conditions. In some cases repeated melts were made in the same crucible by the addition of more pellets. In general, this procedure of repeated melts in the same crucible is not recommended because the crucible sometimes cracked and physical and chemical alteration of the melt was observed, perhaps because of the initiation of reactions which resulted in the deposition of tungsten or volatilization of silica from the melt. It was necessary to break the crucibles to remove the melt. The as-melted samples were X-rayed to identify crystalline phases formed on cooling. Additional heat treatments on as-melted material were carried out in air from 1100°-1600 °C and followed by phase identification using X-ray diffraction and TEM (transmission electron microscopy).

The compositions melted ranged from 20-40 mol% Y_2O_3. This compositional range is centered around the lower temperature eutectic region shown in Fig. 3, which is a modified version of the Y_2O_3-SiO_2 phase diagram without inclusion of the Y2S3 phase. This range covers compositions observed in the intergranular glassy grain boundary phase in as-processed NASA Lewis silicon nitride, assuming the absence of nitrogen within the glass. The exact chemical analysis of this phase is difficult to determine because the EDS (energy dispersive spectroscopy) system on the TEM at NASA Lewis has a Be window, which precludes soft X-rays such as those that arize from O or N. In earlier studies on these materials,[1] no crystallization of nitrided crystalline phases was observed. This may have been due to incomplete crystallization for the given heat treatment of the material or to the inherent difficulties of crystallizing small amounts of glassy material.[7]

The primary glass composition studied was designated GSI. This is the eutectic composition between SiO_2 and $Y_2Si_2O_7$ and is similar to the intergranular glassy grain boundary composition without nitrogen in the as-processed 6Y silicon nitride. The formulation and as-melted composition is

given in Table I. The presence of tungsten will be discussed in the results section. Less than 0.2% nitrogen was found, indicating that little nitrogen was dissolved in the melt as a result of the 50 atm nitrogen overpressure. In addition, a GSII composition was melted containing 52 wt% Y_2O_3 and 48% SiO_2 and a $Y_2Si_2O_7$ composition. The GSZ5 and GSZ10 compositions are the same as GSI with 5 and 10 wt% ZrO_2 added as a nucleating agent. A $2Y_2O_3 \cdot 3SiO_2$, (Y2S3), composition was also melted to determine the stability of this crystalline phase.

Results

In all cases X-ray diffraction of the as-quenched melt indicated partially crystlalization. The diffraction pattern from the as-melted GSI is shown in Fig. 4. The melt is amorphous but with a considerable amount of δ-$Y_2Si_2O_7$ phase present. Even in the case of sol-gel derived glasses at lower temperatures, partial crystallization was observed. Most of the melts contained the δ phase, as would be expected from a rapid quench of the melts. However, in some cases the γ and β phases were observed. A satisfactory explanation cannot be given. The quench obtained in these melts was not a rapid one—estimated to be 270 °/min. The furnace did not permit the more rapid quench that might have been obtained, for example, by pouring into a liquid. Exactly what melting and quenching conditions would result in the formation of the lower temperature polymorphs is not known. In some cases reheating of the melt might contribute to the existence of lower temperature polymorphs at higher temperatures, or the presence of tungsten in the melts may serve as a nucleating agent.

The GSII composition was phase separated on melting, which is expected from the phase diagram. The only exception to the partial crystallinity of the as-melted material was the Y2S3 composition which X-rayed amorphous (Fig. 5). Further experiments are being carried out to confirm this result. The GSZ5 and GSZ10 compositions consisted of β- and γ-$Y_2Si_2O_7$ respectively together with cubic ZrO_2.

The as-melted GSI composition produced β-, γ-, and δ-$Y_2SI_2O_7$ for different melts. Results of heat treatment of these melts are shown in Fig. 6. The X-ray diffraction pattern for a heat treatment of 24 h at 1300 °C is given in Fig. 7. In this case it would appear that all of the δ phase did not transform. In Fig. 8, a TEM micrograph of the GSI composition heat treated for 4 h at 1600 °C shows the presence of SiO_2 glass and δ-$Y_2Si_2O_7$, as expected from the phase diagram. The temperature range of these heat treatments was 1100 °–1600 °C, and times ranged from the initial melt to 43 h. In general, the expected phases were formed, but in some cases metastable phases existed for long periods of time at a given temperature. Cristobalite was not present in sufficient amounts to be observed by X-ray diffraction but was identified by TEM. There was some evidence that the initial crystalline phases formed from the as-quenched melt may have determined the subsequent crystal phases formed. Further work needs to be done to clarify these results.

The results of heat treatment of the GSZ compositions containing 5 and 10 wt% ZrO_2 are shown in Fig. 9. For the GSZ5 composition β-$Y_2Si_2O_7$ was always observed with the cubic ZrO_2. In GSZ10 various phases crystallized including the γ and δ phases. The YS2 and Y2S3 results are shown in Fig. 10. Crystallization of Y_2SiO_5 and δ-$Y_2Si_2Y_7$ at 1600 °C are the phases expected from the phase diagram with no formation of crystalline $2Y_2O_3 3SiO_2$ as shown

in the diffraction pattern in Fig. 11. Crystallization of a polymorph at temperatures above its conversion temperature is unexplained. It may have been due to formation of crystal nuclei on cooling from the melt and subsequent growth during heat treatment. Further crystallization studies are underway to better define the range of temperature stability of these polymorphs.

One of the more troublesome asepcts of this investigation was the presence of tungsten in the melts. Obtaining a satisfactory crucible material was difficult. Materials tried included Pt, Rh, Ir and various alloys of these elements, BN, SiC, and Si_3N_4. None of these materials resulted in melts without dissolution and chemical alteration of the melt or the crucible material. Chemical analysis indicated that tungsten concentrations in the range 0.10–0.80 wt% were dissolved or precipitated in the melts. In some cases, tungsten was deposited on the sides of the crucible or on the melt surface. It is not clear how this formed, but a possible mechamism is oxidation of tungsten to form a vapor which then deposited and decomposed to tungsten. Since little oxidation of tungsten used as shields in the furnace was observed, the concentration of oxygen in the furnace must have been very low. At these temperatures the vapor pressure of tungsten is too low to account for vapor transport of the tungsten metal. It is also possible that tungsten may have dissolved in the melts when liquid.

The TGA scan shown in Fig. 12 for a GSZ5 composition to 1800 °C indicates a 40% weight loss, most likely due to the volatilization of SiO. Melting was indicated at 1750 °C and a crystallization on cooling at 1450 °C. No crystallization or polymorphic inversions were observed on heating nor was there any indication of a glass transition. On cooling again, no polymorphic inversions were observed. Further studies are in progress to see if any crystallization can be detected by heat treatment during a DTA scan or in isothermal holds. DTA results on the GSZ compositions indicated possible crystallization on heating, but these results need to be examined further. It may be of interest to investigate other nucleating agents; however, most would lower the refractoriness of the glassy phase, which would be undesirable in the processing of silicon nitride.

Conclusions

Results of crystallization studies in the Y_2O_3–SiO_2 system have shown that, in general, the expected crystalline phases form when heat treated. It was also found that transformations were sluggish and in some cases phases could exist metastably. When the crystallization studies on the bulk glasses have been completed, the heat-treatment schedules which optimize crystallization will be applied to the 6Y silicon nitride composition to attempt to improve the high-temperature mechanical properties.

Acknowledgement

Research at The Ohio State University was supported on NASA Grant No. NAG 3-824.

References

[1]W. A. Sanders and D. M. Mieskowski, "Strength and Microstructure of Sintered Si_3N_4 with Rare-Earth-Oxide Additions," *J. Am. Ceram. Soc.*, **64** [2] 304–309 (1985).

[2]L. J. Gauckler, H. Hohnke, and T. Y. Tien, "The System Si_3N_4–SiO_2–Y_2O_3," *J. Am. Ceram. Soc.*, **63** [1–2] 35–37 (1980).

[3]K. Liddell and D. P. Thompson, "X-ray Diffraction Data for Yttrium Silicates," *J. Br. Ceram. Trans.*, **85** 17–22 (1986).

[5]E. M. Levin, C. R. Robbins, and H. F. McMurdie, *Phase Diagrams for Ceramists 1969 Supplement,* The American Ceramic Society, Inc., Columbus, OH; Fig. 2388.

[6]W. E. Lee, C. H. Drummond III, G. E. Hilmas, J. D. Kiser, and W. A. Sanders, "Microstructural Evolution on Crystallizing the Glassy Phase in a 6 Weight % Y_2O_3-Si_3N_4 Ceramic," these proceedings.

[4]W. A. Sanders and T. P. Herbill, "Characteristics of Si_3N_4-SiO_2-Ce_2O_3 Compositions Sintered in High-Pressure Nitrogen," *J. Am. Ceram. Soc.,* **66** [12] 835-41 (1983).

[7]R. Raj and F. F. Lange, "Crystallization of Glass (or a Liquid) Segregated in Grain Boundaries," *Acta Met.,* **201** 1993-2000 (1981) and R. Raj, "Morphology and Stability of the Glass Phase in Glass-Ceramic Systems," *J. Am. Ceram. Soc.,* **64** [5] 245-48 (1981).

Table I. Chemical Analysis of GSI

	As Formulated (wt%)	As Melted
SiO_2	40.6	39.94
Y_2O_3	59.4	60.96
WO_3		0.92
N		0.12
		101.94

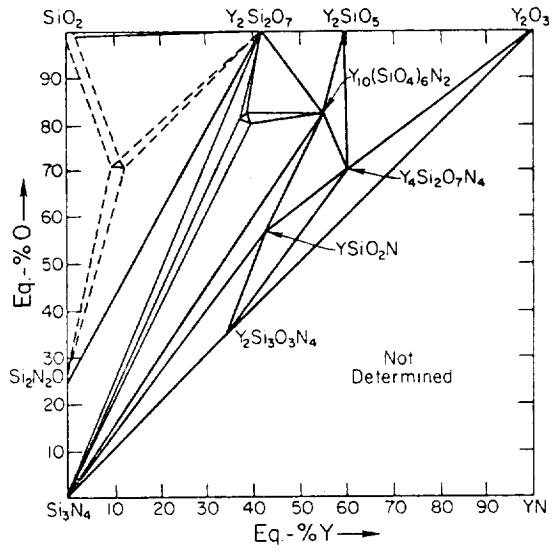

Fig. 1. Isothermal section of the system Si_3N_4-SiO_2-Y_2O_3 at 1500°.

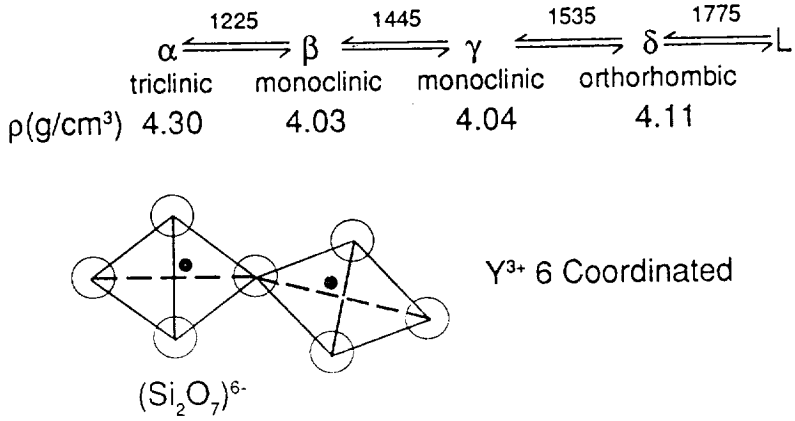

Fig. 2. Polymorphs of $Y_2Si_2O_7$.

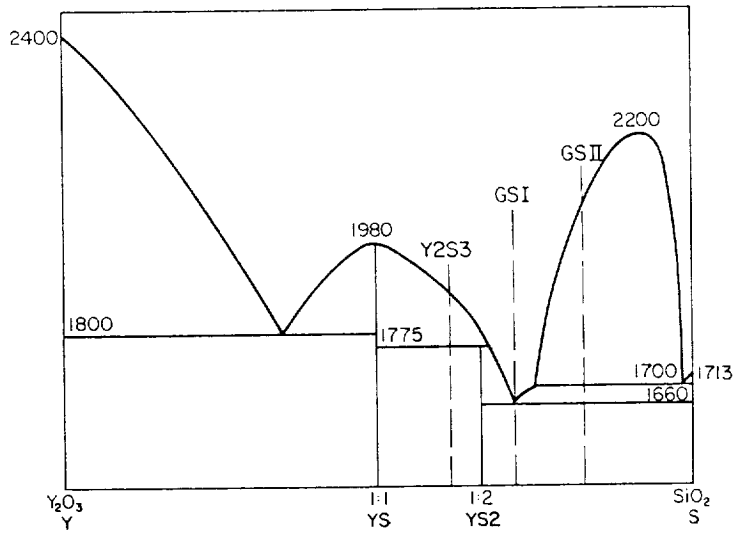

Fig. 3. Y_2O_3-SiO_2 phase diagram.

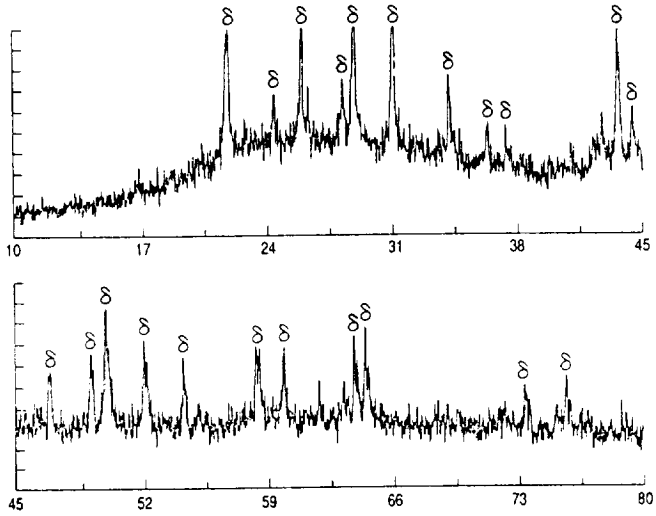

Fig. 4. X-ray pattern of as-melted GSI with δ-$Y_2Si_2O_7$.

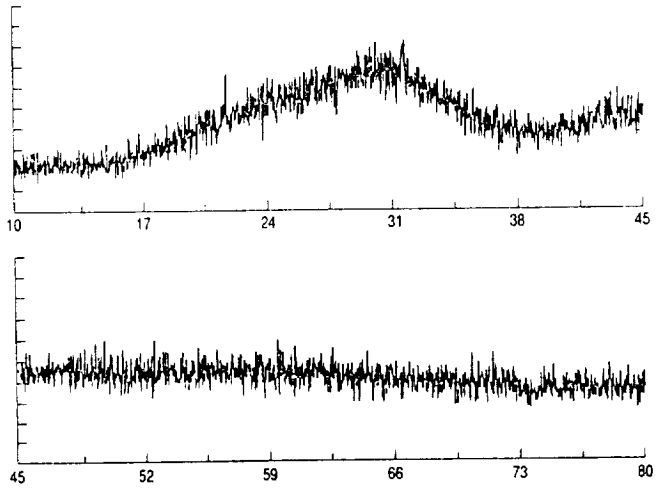

Fig. 5. X-ray pattern of as-melted $2Y_2O_3 \cdot 3SiO_2$.

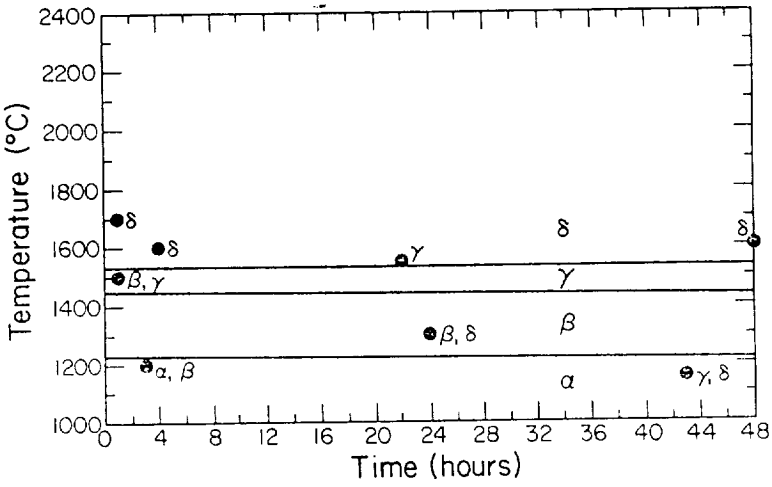

Fig. 6. Heat treatment studies of GSI.

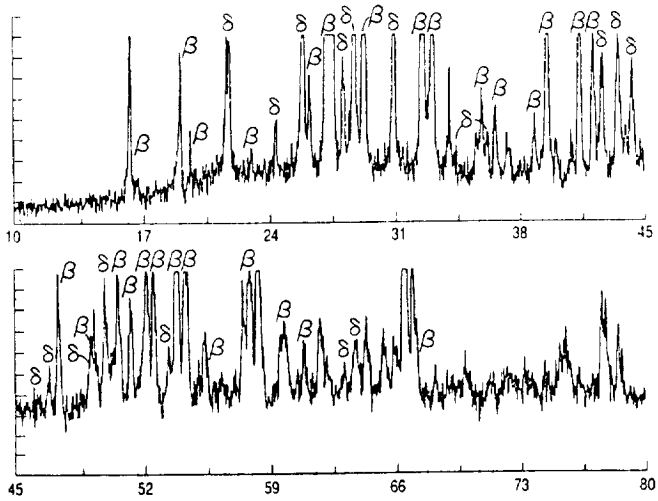

Fig. 7. X-ray pattern of GSI heat treated at 1300 °C for 24 h with β and δ-$Y_2Si_2O_7$.

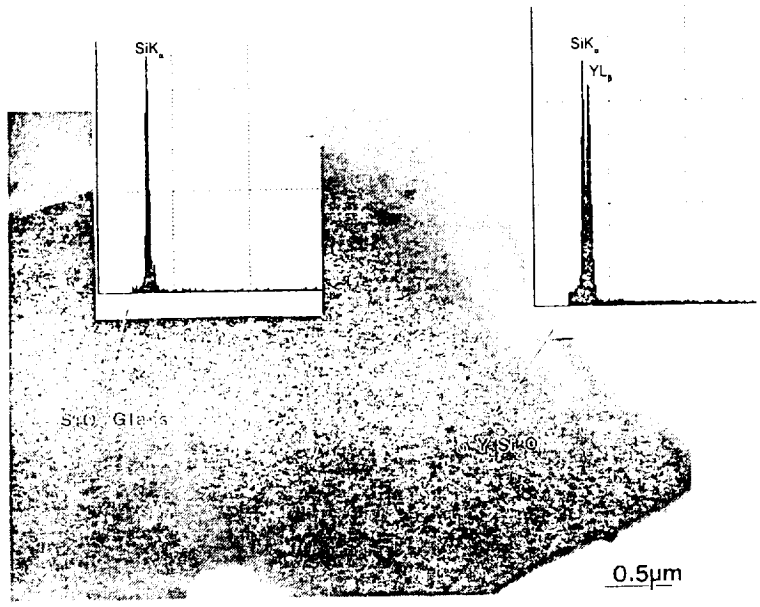

Fig. 8. TEM and AES of GSI heat treated at 1600°C for 4 h.

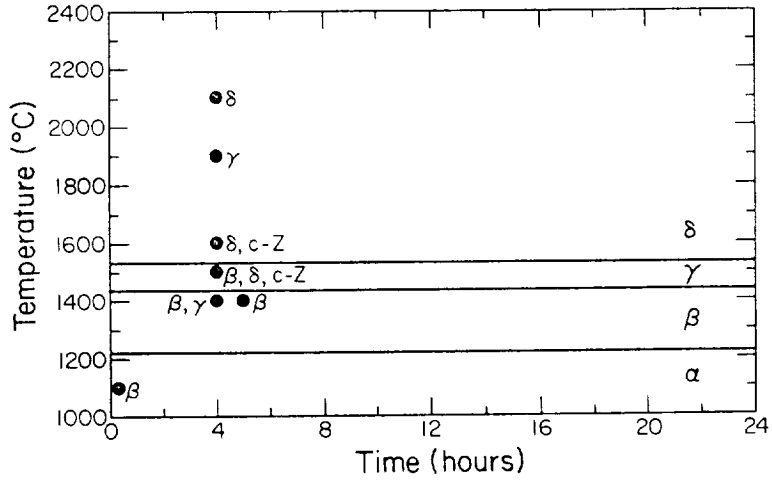

Fig. 9. Heat treatment studies of GSZ compositions.

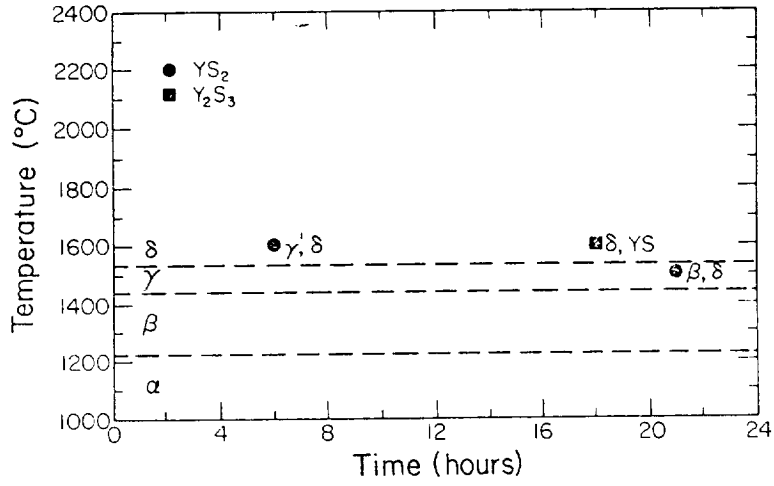

Fig. 10. Heat treatment studies of YS2 and Y2S3 compositions.

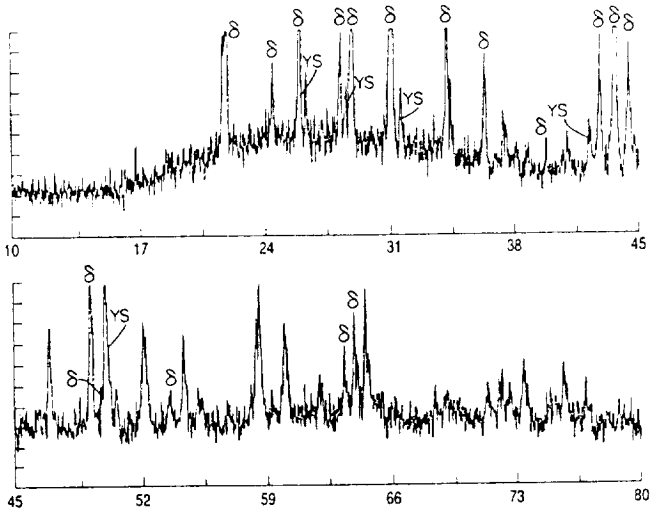

Fig. 11. X-ray pattern of $2Y_2O_3 \cdot 3SiO_2$ heat treated at 1600 °C for 18 h with δ-$Y_2Si_2O_7$ and Y_2SiO_5.

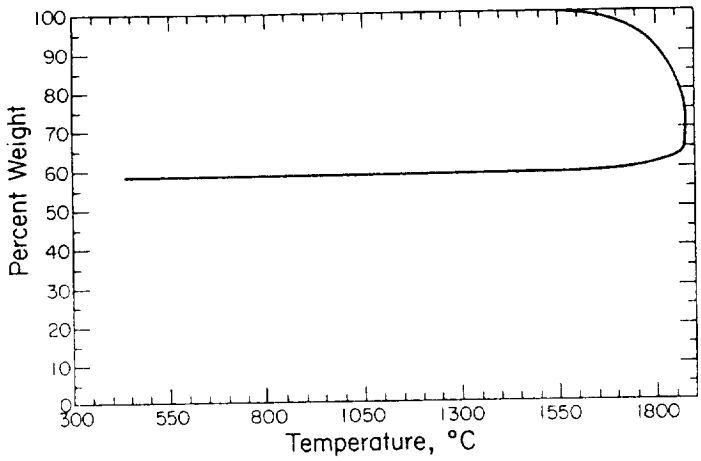

Fig. 12. TGA scan of GSZ5.

Ceram. Eng. Sci. Proc., 9 [9-10] pp. 1355-1366 (1988)

Microstructural Evolution on Crystallizing the Glassy Phase in a 6 Weight % Y_2O_3-Si_3N_4 Ceramic

W. E. LEE, C. H. DRUMMOND III, AND G. E. HILMAS

Department of Ceramic Engineering
The Ohio State University
Columbus, OH 43210

J. D. KISER AND W. A. SANDERS

NASA Lewis Research Center
Cleveland, OH 44135

X-Ray diffraction and analytical electron microscopy have been used to study the crystallization of the grain-boundary glass in a 6 wt% Y_2O_3-Si_3N_4 ceramic. Upon crystallization, high densities of dislocations formed in the Si_3N_4 grains and remained after 5 h at temperature. However, prolonged holds at the crystallization temperature effectively annealed out the dislocations. Other features present in the microstructure are characterized.

Introduction

Microstructural characterizations of liquid-phase sintered Si_3N_4 have frequently been performed using scanning electron microscopy (SEM) to study fracture surfaces and identify failure sites.[1-3] Lattice or structure imaging in the high resolution transmission electron microscope (TEM) has been carried out to detect small quantities of grain boundary glass.[4-5] Other techniques such as energy dispersive spectroscopy (EDS) and energy loss spectroscopy (ELS) in the analytical electron microscope (AEM) have been used to quantitatively determine the chemical constituents of this glassy phase.[6-7] Impurity phases in hot-pressed Si_3N_4 were carefully analyzed by Lou et al.[8] Only recently, however, have microstructural studies been extended to examine the evolution of the microstructure with time and temperature upon crystallizing the glass. Bonnell et al.[9-10] examined crystallization of cordierite ($Mg_2Al_4Si_5O_{18}$) and garnet ($Y_3Al_5O_{12}$) from MgO- and Y_2O_3-containing SiAlONs respectively. In the present work SEM, AEM, and optical microscopy have been utilized to examine the microstructures in NASA-6Y (6 wt% Y_2O_3) composition Si_3N_4 in the as-sintered condition and after a crystallizing heat treatment in N_2 at 1500 °C for times from 5-20 h. We report here the results of AEM analysis.

Experimental

Materials and Sample Fabrication

Details of the starting powders and processing are given in a previous publication[11] and are summarized in Table I. Two series of bars were examined: series A using GTE SN502 Si_3N_4 powder and series B using KBI-AME Si_3N_4 powder. Series A was sintered and crystallized in 25 atm N_2; series B was sintered and crystallized in 50 atm N_2.

Characterization

X-ray diffraction (XRD) of the as-treated surface of the $3 \times 0.56 \times 0.28$ cm bars was carried out using a Philips APD 3600 powder diffractometer. AEM was performed on a Philips 400 EM with an Ortec 500 EDS system. The Be window on the EDS X-ray detector precludes detection of any element lighter than Na so that, unfortunately, neither N nor O could be analyzed with this system. Standard ceramographic grinding and polishing techniques were employed finishing with 3 μm diamond paste. Three-mm diameter TEM disks were ultrasonically cut from 1-mm thick slices of the bars, ground and polished to about 100 μm thickness, dimpled to 20 μm center thickness and ion milled to electron transparency using 5 kV Ar ions. Analysis of X-ray and electron diffraction patterns was facilitated by reference 12 for Si_3N_4 and 13 for $Y_2Si_2O_7$.

Results

X-ray Diffraction

Results of XRD analyses are given in Table II. Series A bars contain detectable amounts of Si_2ON_2 in all cases, even in the as-sintered material. This occurred even though series A had a lower starting SiO_2 content because of contamination during the long milling time (300 h), a higher SiO_2 content in the starting Si_3N_4 powder, and because of possible oxidation of Si_3N_4 upon milling. β-Si_3N_4 was the only other phase found in the as-sintered material but on crystallizing at 1500 °C for 5–20 hours, β-$Y_2Si_2O_7$ peaks were also revealed.

As-sintered series B material was additionally subjected to a bend test in air at 1370 °C before characterization which led to the formation of Y-$Y_2Si_2O_7$* crystals from the glass. After crystallizing treatments of 5 and 10 h at 1500 °C, as in the series A material, only β-$Y_2Si_2O_7$ was formed. However, after 20 h at 1500 °C, only peaks attributable to a α-$Y_2Si_2O_7$ were detected.

General Microstructure

The same general trends in the microstructural features observed in the TEM were seen for both series A and series B material. The main difference was that greater amounts of Si_2ON_2 were apparent in series A (detected by XRD) than in series B samples (not detected by XRD). However, Si_2ON_2 was frequently detected in the TEM when examining series B material even though the amount present must have been below the limits of detectability of the XRD unit (about 5 vol%).

As-sintered 6Y-Si_3N_4: Figure 1 is a bright-field TEM image of a typical area of the microstructure of 6Y material before crystallization consisting of hexagonal β-Si_3N_4 grains in a glassy matrix. The glass appears dark since it contains high atomic number Y which absorbs many of the electrons so that they do not contribute to the transmitted image. An EDS spectrum from the glass is also shown indicating the presence of Y and Si (O and N are not detected with this system). Low densities of dislocations were observed in about 40% of the Si_3N_4 grains examined (e.g. as arrowed in Figure 1). We intend to carry out ELS analysis of the as-sintered glass to determine the N content (if any) and O content.

*There are five polymorphs of $Y_2Si_2O_7$ as described in reference 22.

After 5 h at 1500 °C: All specimens prepared for TEM after this heat treatment were observed to crack on ion milling, a first indication that they were under a large stress. β-$Y_2Si_2O_7$ crystals were seen at the grain boundaries shown as the dark phase in the bright field image of Fig. 2. The EDS spectrum for this phase shows that the Y L_α, L_β doublet peak is just smaller than the Si K_α, K_β doublet peak. Note, however that spectra from this phase must be collected from the edge of the sample away from Si_3N_4 grains to stop X-rays generated from the Si in the Si_3N_4 from reaching the detector, otherwise anomalously high Si peaks result. Figure 3 is a dark-field image where a single reflection from the β-$Y_2Si_2O_7$ has illuminated crystalline regions at the same orientation extending over large areas of the microstructure. It appears that most of the material that was glass before this heat treatment has crystallized at this stage although high-resolution lattice imaging is needed to confirm this.

Figure 4 is a low magnification image of the microstructure. Note the large number of strain fields in the Si_3N_4 grains due to the presence of extensive dislocation networks. Dislocations were observed in about 85% of the grains examined and at much higher densities than in the as-sintered material. Determining the presence of dislocations in a particular grain requires extensive tilting to bring the grain to an orientation at which the dislocation is visible. Work is in progress to quantify the dislocation densities and to analyze their habit planes and Burgers vectors. Figure 5 is a weak-beam dark-field image of some of these dislocations using g = 0002. This technique is frequently used when examining high densities of dislocations in ceramics since it images only the core of the dislocation and removes the problem of overlapping strain fields seen in conventional bright- or dark-field images.

After 10–20 h at 1500 °C: Similar microstructures were observed in these samples as after 5 h at 1500 °C except that the dislocation densities were reduced almost to the level of the as-sintered material (Fig. 6). Specimens did not crack on ion milling.

Other Observations

Several other features were observed in the microstructures using TEM and are worthy of note.

α-Si_3N_4: Rounded grains of α-Si_3N_4 were occasionally observed in all specimens (e.g. arrowed in Fig. 6). Careful analysis of diffraction patterns was required to distinguish these grains from the hexagonally-shaped β-Si_3N_4 grains. The α grains presumably are particles from the original starting powder which did not dissolve during sintering. Observing large numbers of these grains would indicate the need for longer sintering times or higher temperatures although the amounts detected here were small and below the level of detectability of the XRD unit for series B.

Precipitates in the β-Si_3N_4 Grains: Occasionally, small (about 150 nm diameter) crystals were observed inside β-Si_3N_4 grains. EDS analysis of the crystal indicated the presence of silicon, and electron diffraction patterns identified them as being β-SiC, an impurity phase also observed by Lou et al.[8] in their TEM study of hot-pressing Si_3N_4. The crystals are faulted on (111) giving rise to the streaks in the microdiffraction pattern of Fig. 7. The starting powders used in the production of these samples are known to contain about 0.1 wt% C[11] which apparently forms into SiC during the solution-

precipitation sintering process. This observation has practical significance since it is known that carbon impurities reduce the oxidation resistance of Y_2O_3–Si_3N_4 ceramics.[14]

Si_2ON_2 Crystals: Detecting the presence of silicon oxynitride was relatively straightforward in the TEM due to the presence of stacking faults (and occasionally twins) on (100) planes as observed previously by Lewis et al.[15] However, two distinct morphologies of Si_2ON_2 were seen. Commonly, the Si_2ON_2 crystals occurred as long, orthorhombic-shaped grains with the stacking faults running along the long (100) axis of the crystal (Fig. 8). The presence of streaks in the diffraction patterns was a strong indication that the grain was Si_2ON_2. Less common was the appearance of some Si_2OH_2 crystallized with the same morphology as the $Y_2Si_2O_7$ phase, i.e. crystallizing around the Si_3N_4 grains (Fig. 9). This morphology was less inclined to contain stacking faults and so was more difficult to detect. EDS was required to distinguish this from of Si_2ON_2 from $Y_2Si_2O_7$, as was careful analysis of diffraction patterns. In both morphologies, small crystals were seen inside the grains similar to the observation of β–SiC crystals in β–Si_3N_4 noted above. However, preliminary analysis suggests that these crystals are simply Si_2ON_2 microcrystals at a different orientation to the parent grain and not a second phase.

Discussion

Crystallization of the grain-boundary glass to increase the refractoriness of Si_3N_4 ceramics has been intensively studied since the work of Tsuge et al.[16] in the Y_2O_3–Si_3N_4 system. The NASA 6Y composition is chosen to lie in the oxidation-resistant Si_2ON_2–Si_3N_4–$Y_2Si_2O_7$ triangle of the Si_3N_4–SiO_2–Y_2O_3 phase diagram and the microstructural results presented here confirm the presence of these phases along with the occasional impurity grains such as β–SiC (Fig. 7). The increase in dislocation density in the Si_3N_4 grains upon formation of $Y_2Si_2O_7$ after 5 h at 1500 °C was unexpected. Cracking of TEM specimens on ion milling is a clear indication that this material's mechanical properties are adversely affected by this strain. The reduction in dislocation densities with prolonged heating at 1500 °C, however, suggests that the dislocations can be annealed out without difficulty.

The reason for the appearance of dislocations is likely to be associated with a volume difference between the yttrium silicate glass and the first $Y_2Si_2O_7$ crystals formed or volume differences between some of the $Y_2Si_2O_7$ polymorphs. Alternatively, differences in thermal expansion between the various phases may lead to stress in the system. Densities of the polymorphic forms of $Y_2Si_2O_7$ are available but the density of the glass is not. Experiments are currently being performed to determine the density of glasses with this composition. A volume change (increase or decrease) will impose a strain on the Si_3N_4 grains, deforming them and causing dislocations to form. The dislocation microstructures formed in the crystallized material are typical of deformation-induced microstructures seen in other ceramics.[17] According to Liddell and Thompson,[13] α–$Y_2Si_2O_7$ transforms to the β form at 1225 °C which should transform to γ-$Y_2Si_2O_7$ at 1445 °C. Since crystallization was carried out at 1500 °C and γ–$Y_2Si_2O_7$ was never observed, the γ to β transformation must be rapid. Since the β to α transformation did not occur when cooling below the β phase field it, however, must be sluggish. The volume change associated with the only polymorphic transformation to occur (γ to β) is small (0.2%) and so the most likely cause(s) of dislocation formation is (are) a volume change

on crystallization from the glass or differences in thermal expansion behavior. However, as stated above, since the dislocations can be annealed out at the crystallization temperature, their formation need not affect the mechanical properties.

Hayashi et al.[18] note a decrease in flexural strength after crystallization in pressureless-sintered Al_2O_3–Y_2O_3–Si_3N_4 ceramics which they attribute to a change in specific volume of grain boundary phases and difference of thermal expansion coefficients between Si_3N_4 and the crystallized phases.

While a thorough analysis of the dislocations observed in both as-sintered (presumably simple growth defects) and crystallized Si_3N_4 is not yet complete, a few words concerning previous studies of dislocations in this material seem in order. Studies of dislocations in Si_3N_4 are sparse. Evens and Sharp[19] and Butler[20] studied dislocations in hot-pressed and reaction-sintered materials. In both forms most of the dislocations had a <0001>-type Burgers vector, b, although other types of dislocation were present. Consideration of the strain energy associated with various types of dislocation in Si_3N_4[19] indicated that <0001> was the most stable Burgers vector whereas an analysis of dislocation mobility using the Perierls model suggested they would also be the most mobile with $\{10\bar{1}0\}$ as the primary slip plane.

The observation that $Y_2Si_2O_7$ crystallizes at a single orientation (i.e. as a single crystal) over large distances in the microstructure (Fig. 3) is interesting. Similar behavior was seen by Bonnell et al.[10] in garnet ($Y_3Al_5O_{12}$) crystallized in SiAlON grain boundaries but not when cordierite ($Mg_2Al_4Si_5O_{18}$) was crystallized. It is suspected that this behavior is a function of the ease or difficulty of nucleating the second phase; the easier nucleation is the less chance of crystals growing around the Si_3N_4 grains. Since crystallization of $Y_2Si_2Y_7$ is observed around several Si_3N_4 grains. Since crystallization of $Y_2Si_2O_7$ is observed around several Si_3N_4 grains, it seems likely that complete crystallization of all the glass in that area had occurred even though the very thin intergranular regions were not illuminated in dark-field images. High-resolution TEM is planned to determine the extent of crystallization in this material. The crystallization morphologies of the $Y_2Si_2O_7$ polymorphs formed from bulk glass are currently being studied in several complex systems.[21-22]

References

[1]W. A. Sanders and D. M. Mieskowski, "Strength and Microstructure of Sintered Si_3N_4 With Rare-Earth-Oxide Additions," *Ceram. Bull.*, **64** [2] 304–309 (1985).

[2]R. K. Govila, "Uniaxial Tensile and Flexural Stress Rupture Strength of Hot-Pressed Si_3N_4," *J. Am. Ceram. Soc.*, **65** [1] 15–21 (1982).

[3]D. W. Richerson and J. M. Wimmer, "Properties of Isostatically Hot-Pressed Silicon Nitride," *J. Am. Ceram. Soc.*, **66** C-173–76 (1983).

[4]D. R. Clarke, "Direct Observation of Lattice Planes at Grain Boundaries in Silicon Nitride," pp. 433–40 in Nitrogen Ceramics Edited by F. L. Riley (Noordhoff, The Netherlands 1977).

[5]O. L. Krivanek, T. M. Shaw, and G. Thomas, "Imaging of Thin Intergranular Phases by High-Resolution Electron Microscopy," *J. Appl. Phys*, **50** [6] 4223–27 (1979).

[6]D. R. Clarke, N. J. Zaluzec, and R. W. Carpenter, "The Intergranular Phase in Hot-Pressed Silicon Nitride: I, Elemental Composition," *J. Am. Ceram. Soc.*, **64** [10] 601–7 (1981).

[7]S. A. Bradley and K. R. Karasek, "Analysis of Grain Boundaries for Reaction-Bonded Silicon Nitride with Yttria Addition," *J. Mats. Sci. Lett.*, **6** 791–94 (1987).

[8]L. K. V. Lou, T. E. Mitchell, and A. H. Heuer, "Impurity Phases in Hot-Pressed Si_3N_4," *J. Am. Ceram. Soc.*, **61** [9–10] 392–96 (1978).

[9]D. A. Bonnell, M. Ruhle, and T-Y. Tien, "Redistribution of Aluminum Ions During Processing of Sialon Ceramics," *J. Am. Ceram. Soc.*, **69** [8] 623–27 (1986).

[10]D. A. Bonnell, T-Y. Tien, and M. Ruhle, "Controlled Cyrstallization of the Amorphous Phase in Silicon Nitride Ceramics," *J. Am. Ceram. Soc.*, **70** [7] 460–65 (1987).

[11]W. A. Sanders and G. Y. Baaklini, "Correlation of Processing and Sintering Variables With the Strength and Radiography of Silicon Nitride," *Cer. Eng. and Sci. Proc.*, 7 [7–8] 839–59 (1986).
[12]J. V. Sharp, A. G. Evans, and B. Hudson, "Electron Diffraction Data for Silicon Nitride," UKAEA Harwell Report AERE-R7319 (1972).
[13]K. Liddell and D. P. Thompson, "X-ray Diffraction Data for Yttrium Silicates," *Br. Ceram. Trans. J.*, **85** 17–22 (1986).
[14]H. Knoch and G. E. Gazza, "Effect of Carbon Impurity on the Thermal Degradation of an Si_3N_4–Y_2O_3 Ceramic," *J. Am. Ceram. Soc.*, **62** [11–12] 634–35 (1979).
[15]M. H. Lewis, C. J. Reed, and N. D. Butler, "Pressureless-Sintered Ceramics Based on the Compound Si_2N_2O," *Mats. Sci. and Eng.*, **71** 87–94 (1985).
[16]A. Tsuge, K. Nishida, and M. Komatsu, "Effect of Crystallizing the Grain-Boundary Glass Phase on the High-Temperature Strength of Hot-Pressed Si_3N_4 Containing Y_2O_3," *J. Am. Ceram. Soc.*, **58** [7–8] 323–26 (1975).
[17]T. E. Mitchell, "Application of Transmission Electron Microscopy to the Study of Deformation in Ceramic Oxides," *J. Am. Ceram. Soc.*, **62** [5–6] 254–67 (1979).
[18]T. Hayashi, H. Munakata, H. Suzuki, and H. Saito, "Pressureless Sintering of Si_3N_4 with Y_2O_3 and Al_2O_3," *J. Mat. Sci.*, **21** 3501–3508 (1986).
[19]A. G. Evans and J. V. Sharp, "Microstructural Studies in Silicon Nitride," *J. Mats. Sci.*, 6 1292–1302 (1971).
[20]E. Butler, "Observations of Dislocations in β-Silicon Nitride," *Phil. Mag.*, **24** 829–34 (1971).
[21]T. R. Dinger, R. S. Rai, and G. Thomas, "Crystallization Behavior of a Glass in the Y_2O_3–SiO_2–AlN System," *J. Am. Ceram. Soc.*, **71** [4] 236–44 (1988).
[22]C. H. Drummond III, W. E. Lee, W. A. Sanders, and J. D. Kiser, "Crystallization and Characterization of Y_2O_3–SiO_2 Glasses," these proceedings.

Table I. Powders and Processing Conditions

				Sintering			Crystallizing
	Powder	Mill charge (wt%)	Mill time (h)	Temp. (°C)	Time (h)	N_2 pressure (atm)	N_2 pressure (atm)
Series A	Si_3N_4*	95.4	300	2140	1	25	25
	SiO_2†	0					
	Y_2O_3‡	4.6					
Series B	Si_3N_4§	90.0	100	2140	4	50	50
	SiO_2	3.6					
	Y_2O_3	6.4					

*GTE SN 502 99.95% purity, 71.5% α, 1.5% β, 27% amorphous.
†Apache Chemicals Inc., Code 6846, 99.99%.
‡Molycorp. 5600, 99.9%.
§KBI-AME high purity, 99.5%, 83.7% α, 15.7% β, 0.6% Si.

Table II. XRD Results

Crystallizing Time (h)	Phases Present	
	Series A	Series B
0	β-Si_3N_4, Si_2N_2O*	β-Si_3N_4, Y-$Y_2Si_2O_7$†
5	β-Si_3N_4, Si_2N_2O β-$Y_2Si_2O_7$	β-Si_3N_4, β-$Y_2Si_2O_7$
10	β-Si_3N_4, Si_2N_2O, β-$Y_2Si_2O_7$	B-Si_3N_4, β-$Y_2Si_2O_7$
15	β-Si_3N_4, Si_2N_2O, β-$Y_2Si_2O_7$	No data
20	β-Si_3N_4, Si_2N_2O, β-$Y_2Si_2O_7$	β-Si_3N_4, α-$Y_2Si_2O_7$‡

*High SiO_2 content due to contamination from milling media, high SiO_2 in Si_3N_4 powder, and possible oxidation on milling.
†Formed during bend test in air at 1370°C.
‡Identified from 2 peaks only.

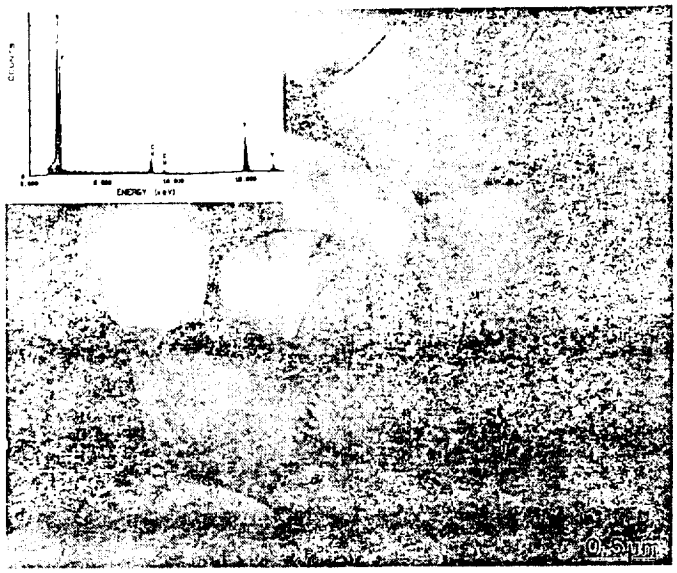

Fig. 1. Bright-field TEM image of as-sintered Si_3N_4. Inset is an EDS spectrum from the glassy phase.

Fig. 2. Bright-field TEM image of Si_3N_4 after crystallization for 5 h at 1500 °C. Inset is an EDS spectrum from $Y_2Si_2O_7$.

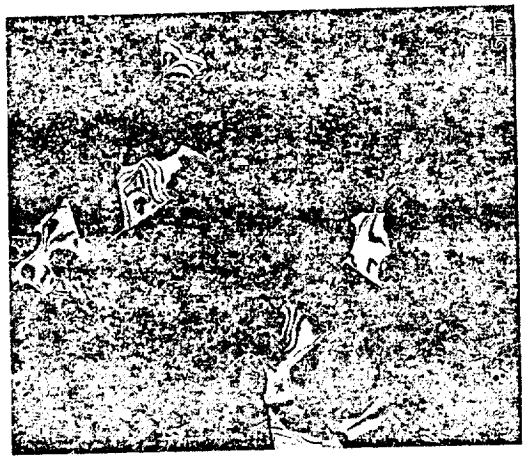

Fig. 3. Dark-field TEM image of β-$Y_2Si_2O_7$ at a single orientation.

Fig. 4. Bright-field TEM image showing large amounts of strain in Si_3N_4 grains after 5 h at 1500 °C.

Fig. 5. Weak-beam dark-field TEM image of a dislocation network in a Si_3N_4 grain.

Fig. 6. Bright-field TEM image showing reduced dislocation density after 20 h at 1500 °C. Arrows indicate α-Si_3N_4 grains.

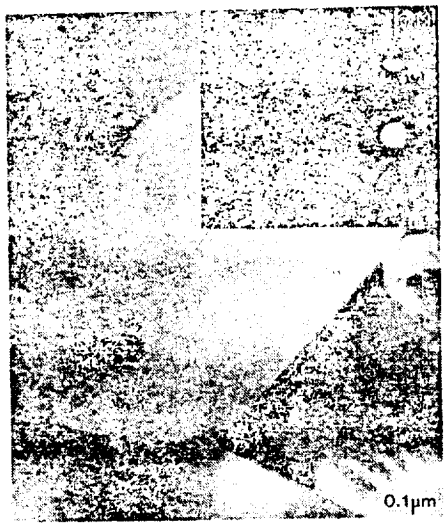

Fig. 7. β-SiC precipitate in Si_3N_4 grain. Inset is a microdiffraction pattern from β-SiC grain with streaking along (111).

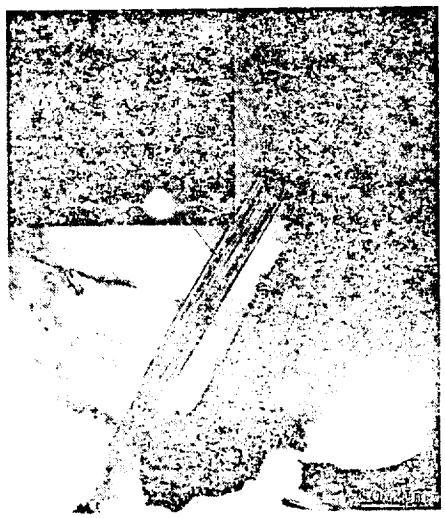

Fig. 8. Orthorhombic Si_2ON_2 grain with stacking faults on (100). Inset difraction pattern showing streaks on (100).

Fig. 9. Si_2ON_2 grain crystallizing around Si_3N_4 grains.